Observation error correlations in IASI radiance data

L.M. Stewart[*], J.Cameron[†], S.L. Dance[*], S.English[†], J.Eyre[†] and N.K. Nichols[*]

Abstract

The optimal utilisation of high resolution satellite observations in Numerical Weather Prediction is being hindered by the mis-specification of their error correlation structure. Variational data assimilation algorithms are run under the assumption of uncorrelated observation errors; yet the contrasting model and satellite observation resolutions lead to errors of representativity, making this assumption unrealistic.

Using a post analysis diagnostic derived from variational data assimilation theory, we quantify cross-channel correlations between IASI (infrared atmospheric sounding interferometer) observations used in the Met Office incremental 4D-Var assimilation scheme. Diagnosed error covariances are given for the pre-processing 1D-Var assimilation and the main 4D-Var assimilation. Comparisons are made with the current operational error covariances.

1 Introduction

Operational data assimilation algorithms often have a variational formulation, where the information provided by the observations and first-guess model background is weighted by the inverse of their respective error covariance matrices. This information is combined in order to produce an accurate, high resolution representation of the current state of the atmosphere for use in Numerical Weather Prediction (NWP); this state is known as the analysis. To ensure an accurate analysis, a good approximation of these error statistics is needed. However, the error characteristics of remotely sensed observation types are not well known, causing forecasting accuracy and observation utilisation to suffer [5], [15], [9].

An incorrect specification of the error covariance matrices can be identified by post-analysis diagnostics, such as those proposed by Hollingsworth and Lönnberg [10]. The method described in [10] uses the statistics of the background innovations, under the assumption that the background errors carry spatial correlations

---

[*]University of Reading, Reading.   Corresponding author email address: l.m.stewart@reading.ac.uk

[†]Met Office, Exeter

while the observation errors do not, to determine the background and observation error variances. However, remotely sensed satellite observations are likely to carry cross-correlations between certain channels, and this conventional method must be modified accordingly [2].

An alternative method that takes account of observation error correlations, is a post-analysis diagnostic proposed by Desroziers et al [7]. Their approach provides a consistency check on the specification of the observation error covariance matrix using the statistics of the background and analysis innovations. The paper demonstrates the success of the method in diagnosing cross-correlations from data which is assumed uncorrelated in the assimilation (i.e, the observation error covariance matrix is set as diagonal) but in reality carries correlations. The work in this report extends the technique to a larger scale problem.

Under the Met Office incremental 4D-Var assimilation scheme, the study aims to identify cross-channel correlations between IASI (infrared atmospheric sounding interferometer) measured brightness temperature errors, using the post-analysis diagnostic as propsed in [7]. Statistics providing information on observation error variances and covariances will be generated using real observations from the current Met Office operational data base (MetDB).

In Section 2, variational data assimilation theory is introduced and the proposed diagnostic is derived. The nature of IASI measurements and the processing they are subject to, is discussed in Section 3. Section 4 is concerned with the application of the diagnostics discussed in Section 2, to IASI measurements from the Met Office operational data base. Results on the calculation of inter-channel IASI observation error covariances for two processing systems are given in Sections 5 and 6. Conclusions and further discussion are given in Section 7.

2 Diagnostics

In 3D-Var data assimilation, observations and background estimates of atmospheric state variables are combined to produce an optimal analysis state, x_a. The background state, x_b, and observation vector, y, are approximations to the true state of the atmosphere, x_t,

$$
\begin{aligned}
y &= Hx_t + \epsilon^o, \\
x_t &= x_b + \epsilon^b,
\end{aligned}
$$

where ϵ^o and ϵ^b are the observation and background errors, respectively, and H is the possibily nonlinear observation operator (or forward model) converting from state space to measurement space. The background and observation error covariance matrices are given by $\mathbf{B} = \mathbb{E}[\epsilon^b(\epsilon^b)^T]$ and $\mathbf{R} = \mathbb{E}[\epsilon^o(\epsilon^o)^T]$, respectively. We assume that the observation and background errors are unbiased and uncorrelated,

$$
\mathbb{E}\left[\epsilon^b\right] = \mathbb{E}\left[\epsilon^o\right] = 0, \tag{1}
$$

$$
\mathbb{E}\left[\epsilon^b\left(\epsilon^o\right)^T\right] = \mathbb{E}\left[\epsilon^o\left(\epsilon^b\right)^T\right] = 0. \tag{2}
$$

The optimal analysis state, x_a, is given by the solution to the cost function

$$J(x) = \frac{1}{2}(x - x_b)^T \mathbf{B}^{-1}(x - x_b) + \frac{1}{2}(y - Hx)^T \mathbf{R}^{-1}(y - Hx),$$

which penalises distance from the background state x_b and the observations y. Also known as the best linear unbiased estimate of the analysis state, x_a is given by

$$\begin{align}
x_a &= x_b + \mathbf{K}(y - Hx_b) = x_b + \delta x_a, \tag{3}\\
\mathbf{K} &= \mathbf{B}\mathbf{H}^T(\mathbf{H}\mathbf{B}\mathbf{H}^T + \mathbf{R})^{-1}, \tag{4}
\end{align}$$

where δx_a is the analysis increment, $\mathbf{H}$ is the linearised version of H, and $\mathbf{K}$ is the Kalman Gain matrix.

Following Desroziers [7], we can write an alternative expression for the analysis state (3) in terms of the background state x_b, the Kalman Gain matrix $\mathbf{K}$ and the innovation vector d_b^o,

$$x_a = x_b + \mathbf{K}d_b^o.$$

The innovation vector d_b^o is the difference between the observations y and their background counterparts Hx_b, and can be described in terms of the observations and background errors,

$$\begin{align}
d_b^o = y - Hx_b &= Hx_t + \epsilon^o - Hx_b \\
&\approx \epsilon^o + \mathbf{H}(x_t - x_b) \\
&\approx \epsilon^o + \mathbf{H}\epsilon^b. \tag{5}
\end{align}$$

Similarly, the analysis innovation vector is given by the differences between the observations y and their analysis counterparts Hx_a,

$$\begin{align}
d_a^o = y - Hx_a &= y - H(x_b + \mathbf{K}d_b^o) \\
&\approx y - \mathbf{H}x_b - \mathbf{H}\mathbf{K}d_b^o \\
&\approx (\mathbf{I} - \mathbf{H}\mathbf{K})d_b^o \\
&\approx \mathbf{R}(\mathbf{H}\mathbf{B}\mathbf{H}^T + \mathbf{R})^{-1}d_b^o. \tag{6}
\end{align}$$

By taking the expectation of the cross product of the analysis and background innovations, and using the assumpion of uncorrelated errors (2), we find a statistical approximation for the observation error covariances,

$$\begin{align}
\mathbb{E}\left[d_a^o(d_b^o)^T\right] &\approx \mathbb{E}\left[\mathbf{R}(\mathbf{H}\mathbf{B}\mathbf{H}^T + \mathbf{R})^{-1}d_b^o(d_b^o)^T\right] \\
&\approx \mathbf{R}(\mathbf{H}\mathbf{B}\mathbf{H}^T + \mathbf{R})^{-1}\mathbb{E}\left[(\epsilon^o + \mathbf{H}\epsilon^b)(\epsilon^o + \mathbf{H}\epsilon^b)^T\right] \\
&\approx \mathbf{R}(\mathbf{H}\mathbf{B}\mathbf{H}^T + \mathbf{R})^{-1}\left(\mathbb{E}\left[\epsilon^o(\epsilon^o)^T\right] + \mathbf{H}\mathbb{E}\left[\epsilon^b(\epsilon^b)^T\right]\mathbf{H}^T\right) \\
&\approx \mathbf{R}(\mathbf{H}\mathbf{B}\mathbf{H}^T + \mathbf{R})^{-1}\mathbf{R}(\mathbf{H}\mathbf{B}\mathbf{H}^T + \mathbf{R}) \\
&\approx \mathbf{R}. \tag{7}
\end{align}$$

The relation (7) should be satisfied provided the matrix $\mathbf{R}(\mathbf{H}\mathbf{B}\mathbf{H}^T + \mathbf{R})^{-1}$ is consistent with the exact observation and background error covariances. This diagnostic can be used as a consistency check to ensure the observation error covariances are correctly specified in the analysis. Similar diagnostics can be generated to check the background error covariances in observation space, $\mathbf{H}\mathbf{B}\mathbf{H}^T$, the analysis errors covariances, $\mathbf{H}\mathbf{A}\mathbf{H}^T$ where $\mathbf{A} = (\mathbf{B}^{-1} + \mathbf{H}^T\mathbf{R}^{-1}\mathbf{H})^{-1}$, and the sum of the observation and background error covariances, $\mathbf{R} + \mathbf{H}\mathbf{B}\mathbf{H}^T$ [7].

3 Processing

3.1 IASI measurements

IASI data is an important component of the global observing system used in NWP, and is used successfully in conjunction with other satellite radiance observations (e.g. AMSU-B microwave sounding of temperature and water vapour), and other observation types (e.g. radiosondes and satellite winds). The IASI instrument is an infrared Fourier transform spectrometer that measures the infrared radiation emitted by the earth's surface and atmosphere [3]. The first IASI instrument was launched on the MetOp-A satellite in 2006 as part of the EUMETSAT European Polar System (EPS). It's spectral interval of 645-2760cm^{-1} is divided into three bands and sampled by 8461 channels at a resolution of 0.5cm^{-1}. Band one, from 645-1210cm^{-1}, is used primarily for temperature and ozone sounding, band two (1210-2000cm^{-1}) for water vapour sounding and the retrival of N_2O and CH_4 column amounts, and band three (2000-2760cm^{-1}) for temperature sounding and the retrival of N_2O and CO column amounts.

IASI measurements of radiances, r, are expressed as black-body equivalent brightness temperatures, T, through Planck's function

$$r = \frac{2h\nu^3 c}{\exp\{\frac{hc\nu}{kT}\} - 1},$$

where k is Boltzmann's constant, h is Planck's constant, c is the speed of light and ν is the wavenumber. Any processing IASI observations are subject to is performed with respect to their equivalent brightness temperatures.

Brightness temperature measurement errors can be attributed to three sources: forward model error, instrument noise, and representativity error. The former two are likely to be independent with channel selection, but the latter may be correlated for certain channel pairs. However, the current assumption in NWP is that all observation errors are independent, i.e, $\mathbf{R}$ is a diagonal matrix.

Instrument manufacturers provide the error associated with an instrument reading from a black body at $280K$; known as the neδt value. Although the error in the measured radiance value is assumed invariant under scene temperature (average brightness temperature), the corresponding brightness temperature is not. Therefore for each channel used in the assimilation, the mean brightness temperature measurement must be calculated and the neδt value adjusted accordingly. The converted neδt value will be the error associated with an instrument reading at the channel wavelength, from a black body at the mean brightness temperature. Regular calibrations at different wavelengths ensure that instrument noise for different channels is uncorrelated.

The forward model error includes errors associated with discretization of the radiative transfer equation and mis-representation of the gaseous contributors in certain channels. Again these errors are likely to be uncorrelated between channels.

Representativity error is present when the observations can resolve spatial scales or features that the model cannot. If observations are used at a higher spatial frequency than the model resolution, then they will be affected by correlated representativity error because the model will be unable to represent the finer scale spatial structure given by the observations. Operationally, no observations are assimilated at a higher density than the model resolution and data thinning procedures such as superobbing [1] are used to compensate for the loss of information. Also if the model resolution is too large to represent a small scale physical feature as represented in the observation, then correlated representativity errors will be present. For example, the forecast model may be unable to represent accurately a complex humidity structure at its current resolution, leading to correlations in the errors between channels sensitive to water vapour.

Any pre-processing the observations are subject to will generate errors. For example, if we eliminate all observations affected by clouds and some residual cloud passes through the quality control, then one of the assimilation assumptions is violated and the cloudy observations will contaminate all the channels which are influenced by the cloud.

3.2   1D-Var retrievals

In any assimilation procedure, we wish to only assimilate observations that provide useful information about the state variables. Those which are affected by significant errors or unmodelled parameters, such as cloud, may provide very little useful information or even cause problems with convergence rates. Therefore before IASI observations are passed to the incremental 4D-Var assimilation, they are subject to pre-screening and quality control.

IASI has the potential to provide observations in 8461 channels, but only observations from a subset of 314 are used. These 314 channels are chosen based on their information content (degrees of freedom of signal) using the automatic channel selection algorithm of Rodgers [13], with some manual intervention to ensure a robust selection. Further details on channel selection are given [4]. Before the observations from the pre-determined 314 channels are assimilated in 4D-Var, they are passed through the Observation Processing System (OPS).

IASI measured brightness temperatures are fed into the OPS and processed using a code specifically written for satellite measurements. This code, known as the SatRad code, implements a 1D-Var assimilation on the bias-corrected brightness temperature measurements, y, and an accurate first-guess model-profile from a short range forecast, x_b. The solution is the state vector x that minimises the cost function,

$$J(x) = \frac{1}{2}(x - x_b)^T \mathbf{B}^{-1}(x - x_b) + \frac{1}{2}(y - Hx)^T \mathbf{R}^{-1}(y - Hx),$$

where H is the observation operator transforming from state space to measurement space, $\mathbf{B}$ is the background error covariance matrix and $\mathbf{R}$ is the observation

Figure 1: Path of IASI observations

error covariance matrix. The observation operator H is comprised of a Radiative Transfer for TIROS Operational Vertical Sounder (RTTOV) radiative transfer model [14]; it accurately predicts brightness temperatures given first-guess model fields of temperature and humidity on 43 fixed pressure levels between 0.1 and 1013hPa, as well as surface air temperature, skin temperature and surface humidity.

The OPS has two main functions: the first is quality control on the brightness temperature measurements, and the second is providing updated first-guess model fields. The assimilation performs a local analysis of the model state at the location of every satellite observation; an observation is suitable for 4D-Var assimilation if its 1D-Var analysis generates a good convergence and a suitable a posteriori cost [16]. Each observation has an associated cost which is scaled to be ideally 1, and if the distribution of the costs about 1 was plotted, the quality control procedure would be equivalent to eliminating those observations whose costs lie in the tails of

the distribution.

Unsuitably high costs and slow convergence are caused by inconsistencies between the background and the observations; for example, if the background assumes a clear sky but the observation is affected by cloud. If we consider the prior and likelihood distributions of the background and the observations, then the 1D-Var assimilation finds the solution with maximum probability that satisfies both the background and the observation distribution. If the distributions are highly overlapping, then the solution state will exist with a high probability; if the distributions have a small overlap then the solution state is improbable, convergence to it will be slow, and its cost will be high. Identifying and eliminating these observations in 1D-Var enables a stable and fast convergence in 4D-Var.

The 1D-Var assimilation also provides estimates of the atmospheric variables not represented in 4D-Var. The control vector in 4D-Var is comprised of a subset of the full state vector variables, and those variables, such as skin temperature, which are not included are unmodifiable. It is therefore crucial to the success of the assimilation that these variables are accurately specified prior to the 4D-Var assimilation. For example, radiance observations provide information on all atmospheric variables and a poorly specified skin temperature is unchangeable, so therefore the control vector variables will be fit incorrectly to the observations. The full state vector is used in the 1D-Var assimilation, and the analysis values of those variables not present in the control vector are passed to 4D-Var. A schematic of the path of IASI observations is shown in Figure 1.

When the 1D-Var assimilation is performed in the OPS, the forward model is separately fitted to each individual column of observations, so the position of the observations, and hence any resolution conflicts, is already determined. Therefore, it can be argued that the representativity errors will appear in the background matrix B, and so correlations in representativity error within the observation error covariance matrix R will be low. Hence, from the OPS diagnostics (7) we expect any error correlations to be mainly attributed to instrument noise and forward model error.

3.3   Incremental 4D-Var assimilation

The Observation Processing System produces a quality controlled subset of brightness temperature measurements suitable for assimilation in the Met Office incremental 4D-Var assimilation system [12]. As with the 1D-Var procedure, 4D-Var assimilation aims to minimise a cost function penalising distance from the solution state to the observations, y_i^o, and the first-guess background profile,x^b,

$$J(x_0) = \frac{1}{2}(x_0 - x^b)^T \mathbf{B}^{-1}(x_0 - x^b) + \frac{1}{2}\sum_{i=0}^{n}(H_i(x_i) - y_i^o)^T \mathbf{R}_i^{-1}(H_i(x_i) - y_i^o), \quad (8)$$

subject to a nonlinear model

$$x_i = M(t_i, t_0, x_0).$$

The background and observation error covariance matrices are given by $\mathbf{B}$ and $\mathbf{R}_i$, respectively, and the forward model is given by H_i.

The solution to the full cost function is expensive to solve, and hence an incremental approximation to the problem is considered instead [11]. The incremental 4D-Var algorithm approximates the solution of the full nonlinear cost function by performing a series of minimisations of the approximate quadratic cost functions. The algorithm generates an optimal analysis increment, which is used to update the solution state at the start of the assimilation time window. From this starting state, the nonlinear model is run over the time window to generate a forecast. The forecast model fields are outputed at the model grid points at pre-determined times, and can be interpolated in time and space to the observation locations.

In the 4D-Var assimilation, all observation information is fitted to the resolution provided by the model, and so correlated representivity errors are expected to be wholly contained in $\mathbf{R}$.

4   Application of diagnostics to IASI observations

The objective of this paper is to use the background and analysis increment statistics generated from the assimilation of IASI data, to provide a consistency check on the observation error covariances used in the assimilation. We will generate the post-analysis diagnostic (7) in two stages: firstly using the analysis output from the OPS and then using the analysis output from the incremental 4D-Var assimilation. The suitability of our diagnostics (derived from 3D-Var assimilation theory) for 4D-Var assimilation is shown in Appendix B.

As previously mentioned, before satellite radiances are assimilated into 4D-Var, they are passed through the OPS for quality control. Within the OPS, a 1D-Var assimilation is performed on the equivalent brightness temperatures and a first-guess background, producing an analysis retrieval. The first set of statistics will be generated using the background, d_b^o, and analysis, d_a^o, innovations from the 1D-Var assimilation.

The initial OPS run analyses those atmospheric quantities not present in the 4D-Var state vector, and passes them to 4D-Var with a quality controlled set of brightness temperatures; these are used to produce an optimal analysis increment. Along with the forecast value at the start of the time window, the increment is run through the Unified Model (UM) [6] over the time window to generate an analysis trajectory. Using the same observation set, the analysis fields can be passed back through OPS (the second OPS run), only this time as the background input. This allows us to use the background innovations generated by OPS as the d_a^o innovation statistics for the 4D-Var assimilation (see Figure 2).

Clearly we only want to generate our statistics from those observations that are
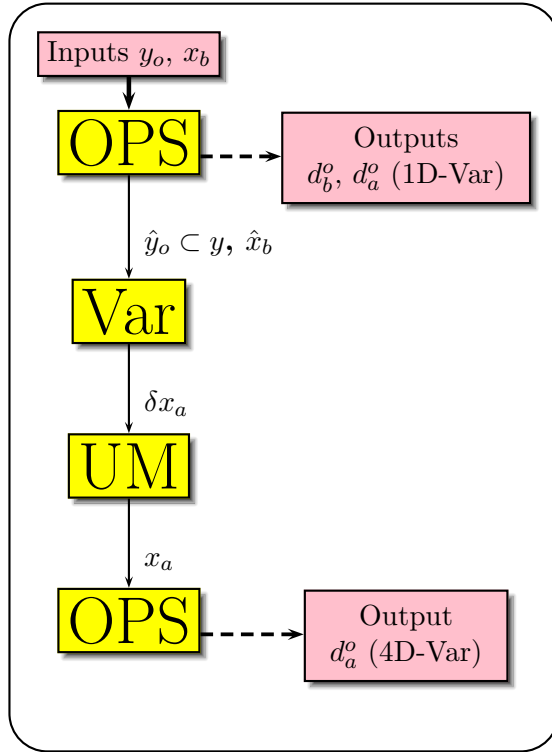
Figure 2: Assimilation process

deemed suitable to process in the Var system, i.e, those that pass the OPS quality control. These are easily identifiable since OPS assigns all observations a quality control flag value: 0 if the observation is passed to Var, 1 if the observation was accepted by Var but spatially thinned out, and > 1 if the observation was rejected. However, the observations passed to Var in the second OPS run will not be the same as those passed in the initial run, because the backgrounds are different. To ensure that the same observations are used to generate the d_b^o innovations in the initial OPS run and the d_a^o innovations in the second OPS run, we match observations using their latitude and longitude values.

All assimilations will be performed using only clear sky, sea surface IASI observations. Observations will be from both day and night time, with the exception of daytime observations from shortwave channels which will be eliminated. We are interested in the correlations between channels used in (i) the 1D-Var assimilation in OPS (183 channels), (ii) the 4D-Var assimilation (139 channels).

For each channel i, we compute the observation error covariance with channel j by averaging the product of the background and analysis innovations over the total number of observations used in the assimilation N,

9

$$
\begin{aligned}
R(i,j) &= \frac{1}{N}\sum_{k=1}^{N}\{(d_a^o)_i\,(d_b^o)_j\}_k - \left(\frac{1}{N}\sum_{k=1}^{N}\{(d_a^o)_i\}_k\right)\left(\frac{1}{N}\sum_{k=1}^{N}\{(d_b^o)_j\}_k\right) \\
&= \frac{1}{N}\sum_{k=1}^{N}\{y_i^o - y_i^a\}_k\{y_j^o - y_j^b\}_k \\
&\quad - \left(\frac{1}{N}\sum_{k=1}^{N}\{y_i^o - y_i^a\}_k\right)\left(\frac{1}{N}\sum_{k=1}^{N}\{y_j^o - y_j^b\}_k\right),
\end{aligned}
\tag{9}
$$

where y_i^o is the brightness temperature value in channel i, and y_i^a and y_i^b are the analysis and background counterparts, respectively. We subtract the mean innovation values to ensure our diagnostic is unbiased.

This diagnostic is only an approximation of the observation error covariance matrix, and by construction may not be symmetric. Since an error covariance matrix is required to be symmetric positive definite, we can consider the symmetric component of our diagnosed matrix

$$
\mathbf{R}_{\text{sym}} = \frac{1}{2}(\mathbf{R} + \mathbf{R}^T).
\tag{10}
$$

5   Results: OPS

The computations (9) are performed on the analyses produced by the 1D-Var assimilation of data from the 17th July 2008 at 00z, 06z, 12z and 18z, within the Observation Processing System. The total number of observations used to produce the statistics was 27,854; 9,131 of which were suitable for use in the 4D-Var assimilation and 18,723 were thinned out. Figure 3 shows the global location of all the observations used in the OPS, and the size of their background innovations for (a) channel 1 (sensitive to temperature) and (b) channel 279 (sensitive to water vapour).

Figure 4 (a) shows the operational observation error variances used in the 1D-Var assimilation (black line), the error variances diagnosed by (7) (red line), and the instrument noise squared (blue line), for all the 183 channels used in the OPS. The channels numbers correspond to the index of the MetDB channel used in OPS, i.e, MetDB channel number 1 has OPS channel index 0 (the first channel used in OPS) and MetDB channel 280 has OPS channel index 182 (the last channel to be used in OPS). Figure 4 (b) shows a typical IASI spectrum for all 314 channels; the channels used in OPS are highlighed by the red asterisks (the full list of corresponding channel numbers and indices can be found in Appendix A).

The structure of the operational and diagnostic error variances is very similar. The diagnosed error variance is significantly lower than the current operational variance for all channels; and in most channels, the diagnosed error variance is also lower than the instrument noise squared. The error standard deviations used in the OPS (square root of the variances) are comprised of the instrument noise, plus forward
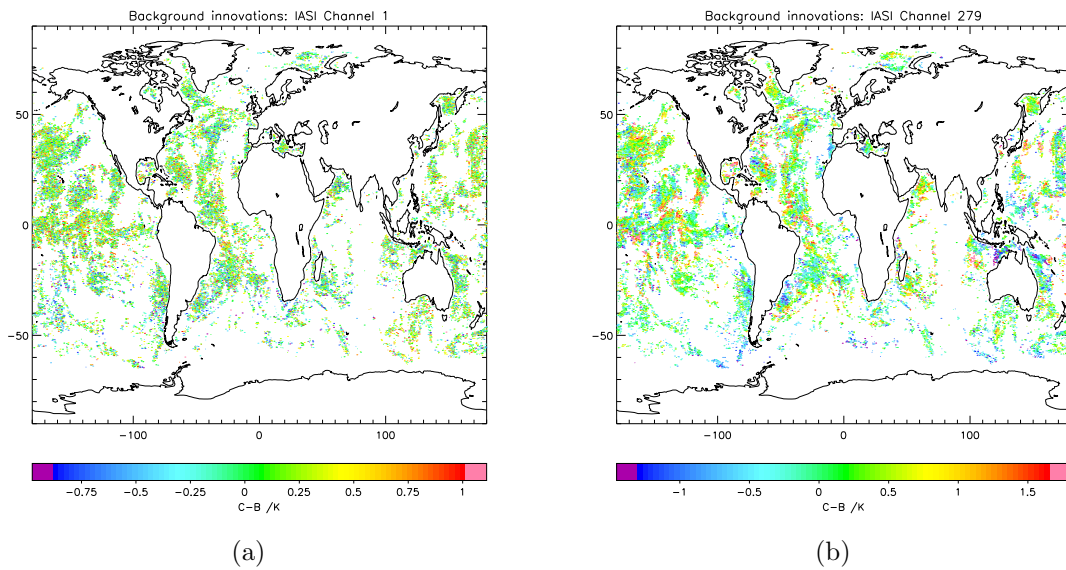
Figure 3: Global location and background innovation value (degrees Kelvin) for observations in: (a) channel 1, (b) channel 279
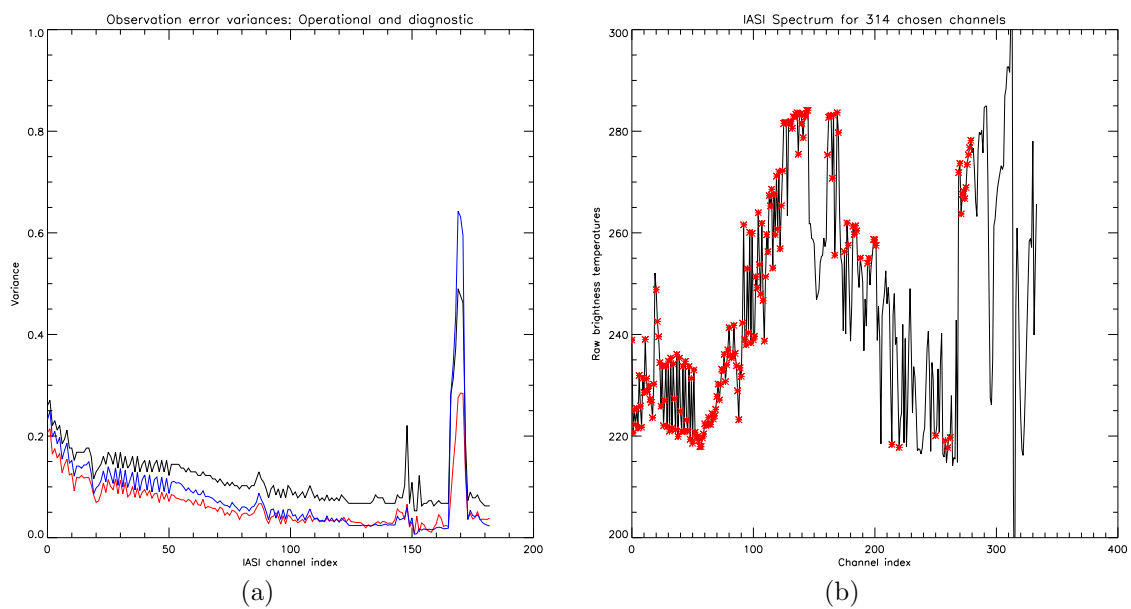

Figure 4: (a) Operational error variances (black line), diagnosed error variances (red line), and instrument noise squared (blue line); (b) channels used in OPS (red crosses) on a typical IASI spectrum (black line)
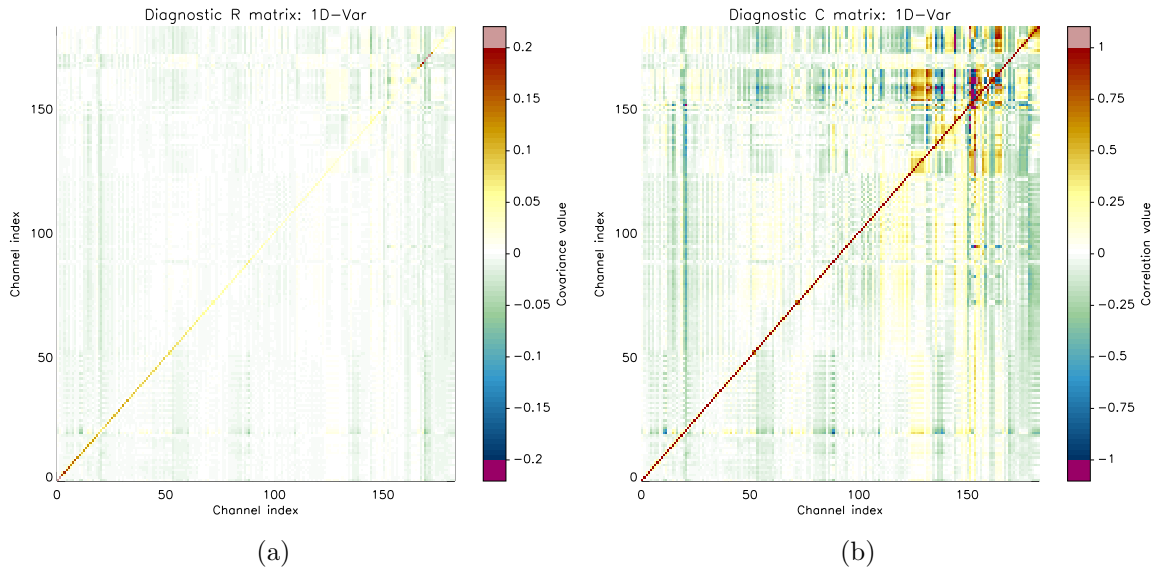
Figure 5: (a) Diagnosed observation error covariances for OPS; (b) diagnosed observation error correlations for OPS

model error of 0.2 and a small error for mis-specification of trace gases, and therefore the error variances should be greater than the instrument noise squared. In channels with OPS index 168 - 171, the instrument noise squared is greater than the operational observation error variance. This is unusual, and suggests that different average raw brightness temperatures may have been used in the conversion of the neδt value for different scene temperatures. The high peaks for the OPS indexed channels 145 - 180 correspond to error variances in channels highly sensitive to water vapour.

Figure 5 shows the observation error covariances and correlations, respectively, for the 183 channels used in the OPS. The error covariance plot is heavily diagonally dominant; the diagonal values on Figure 5 correspond to the values plotted on the red line in Figure 4, and the peaks are represented by the darker colours towards the top of the diagonal. Small covariance values exist between some of the higher indexed channels, which are represented by the darker colours in the top corner of the observation error correlation plot.

The correlations are relatively weak between channels with OPS index under 120, with the exception of channel 20 (MetDB number 21). However, channel 20 is a high-peaking channel in the temperature sounding band, which is not used in the 4D-Var assimilation because of the stratospheric ringing of its innovations. The correlation structure in the higher OPS indexed channels is not uniformly symmetric, suggesting that the iterative procedure for updating the error variances (as proposed by Desroziers [7]) could be beneficial. However, the variance and covariance values are very small, and we must be wary of the accuracy of large correlation values.
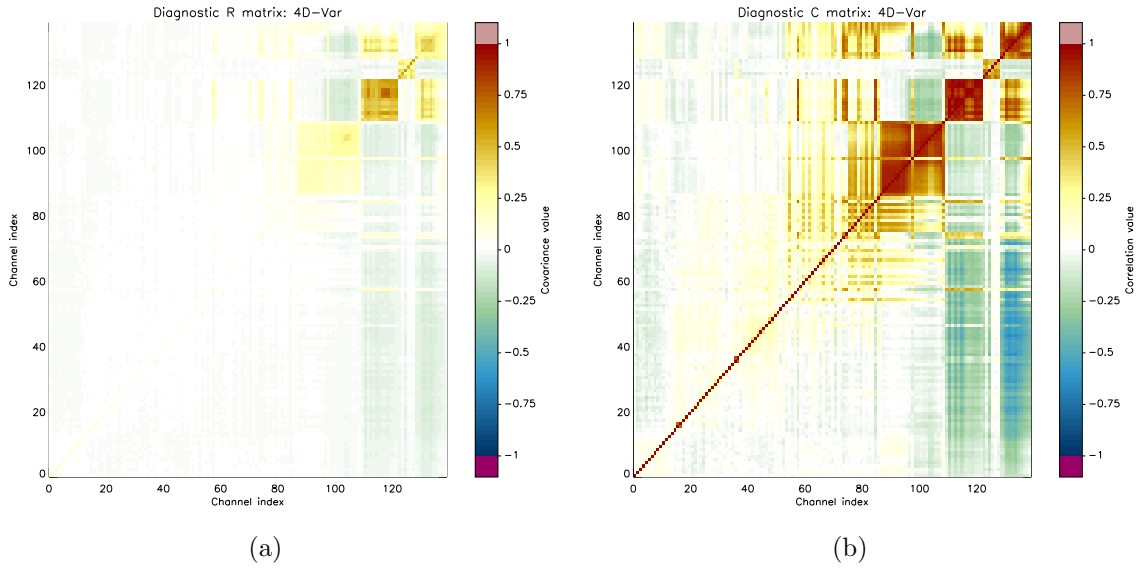
Figure 6: (a) Diagnosed observation error covariances for 4D-Var; (b) diagnosed observation error correlations for 4D-Var

6 Results: 4D-Var

Since the observation error covariance matrix used in the OPS is comprised mainly of instrument noise and forward model error, it is expected to contain a low level of correlation and be diagonally dominant. However, the observation error covariance matrix used in the 4D-Var assimilation, additionally comprises of errors of representativity, and is therefore expected to contain a higher level of correlation.

The computations described in (7) are performed on the analyses produced by the 4D-Var assimilation of data from the 17th July 2008 at 18z. The total number of observations used to produce the statistics was 2,073 (of the total 6,539 observations used in the OPS). The statistical results from the assimilation identify strong correlations bewteen channels highly sensitive to water vapour. The operational error variances used in the 4D-Var assimilation are found to be significantly larger than those diagnosed from the computations.

Figure 6 shows the observation error covariances and correlations, respectively, for the 139 channels used in 4D-Var. Compared to Figure 5, the variances are notably larger (up to 0.8 in Var channel 263) and off-diagonal covariances are more prevalent. There are four significant block structures of covariance centered around the diagonal: the first for Var channels between 124-171 (index 86-108) sensitive to surface emissivity (window channels), the latter three for Var channels 176-202 (index 109-121), 215-263 (index 122-127), and 270-280 (index 128-138), respectively, sensitive to water vapour. The block structure implies the channels in each block have highly correlated errors.

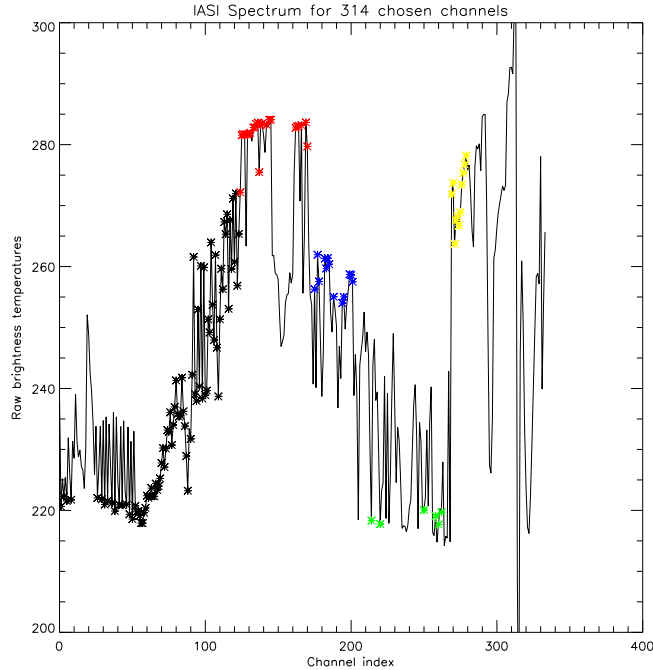By examining the IASI spectrum for the channels used in Var (Figure 7) and

Figure 7: Channels used in 4D-Var on a typical IASI spectrum: Var channel indexed 0-85 (black), 86-108 (red), 109-121 (blue), 122-127 (green), 128-138 (yellow)

the table of spectral information (Appendix A), we see that the channels that carry significant correlations between them, have similar spectral properties. For example, the channels between 215-263 used in Var (index 122-127) have typical brightness temperature measurements between 217-222K, and a Q jac peak at 208.16hPa. Var channel blocks 176-202 and 270-280 also have similar brightness temperature measurements and a strong correlation structure in Figure 6.

The block structures can be seen more clearly in the observation error correlation plot (Figure 6 (b)), which also shows bands of correlation surrounding the first, and largest, block structure. The correlation bands are present in channels sensitive to water vapour. Using the summed Q jac value (see Appendix A) as a measure of the sensitivity of a channel to water vapour: channel index 60 (Var channel 98) has a value of 0.113 and a significant band of correlation, while channel index 61 (Var channel 99) has a value of 0.022 and a near zero correlation value with the surrounding channels. The largest summed Q jac values are found in the low-peaking Var channel blocks 176-202 and 270-280 (up to 1.000 in channel 272).

Both error matrices in Figure 6 are predominantly symmetric, with the exception of the correlations between the water vapour channels in channel index blocks 109-121 and 128-138. This non-symmetric feature could be attributed to the violation of the assumption that the observation errors are correctly specified when generating the statistics (7). Our results suggest observation errors are correlated between certain channels, but the observation error covariance matrix used in 4D-Var is diagonal. This emphasises the need to include a correlation structure in the error covariance matrix.
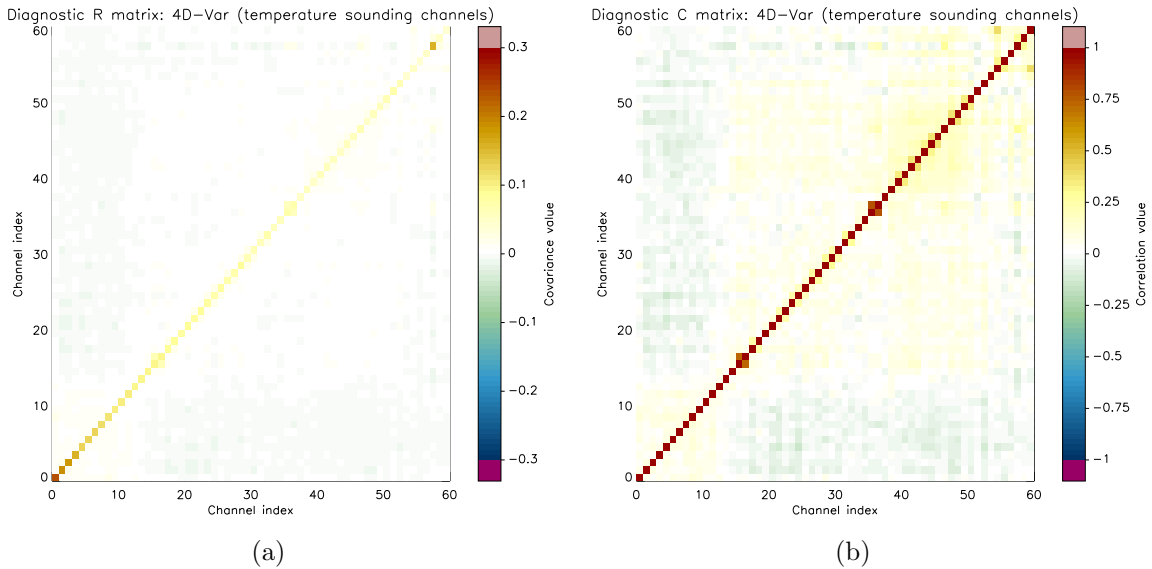
Figure 8: (a) Diagnosed observation error covariances in temperature sounding channels; (b) diagnosed observation error correlations in temperature sounding channels

Although correlations are largest in those channels highly sensitive to water vapour, a level of correlation is also present in the channels used in temperature sounding. Two fainter blocks of correlation centred on the diagonal can be distinguished for channel indicies 0-10 (Var channels 2-42) and 11-50 (Var channels 44-88) (Figure 8); channels 14 and 24 are highly correlated with their neighbouring channel within these blocks. Many of the channels within these blocks are adjacent to each other, and the differences in the data provided can be used to capture fine scale information on the atmospheric profiles; it is therefore desirable to include any diagnosed correlation structure in an attempt to lower the operational error variances and hence retain more information.

Figure 9 and 10 show some of the important off-diagonal structure in more detail. Figure 9 compares the observation error variances used in 4D-Var with those diagnosed from the statistics in this report, and the first lower off-diagonal covariance value. For all channels, the diagnosed variances are considerably less than those being used operationally, implying an overestimation of observation error variances in 4D-Var. However, when we look at the first off-diagonal covariance value, we can see why this overestimation might take place. For several Var channels indexed 86 upwards, the first off-diagonal covariance value is very close in size to the diagonal variance value, therefore if this value, and additional off-diagonal covariances, were to be ignored, the observations would be over-weighted in the analysis. It is therefore necessary to inflate the error variances if we choose to ignore off-diagonal covariances [5].

The size of the off-diagonal covariances and correlations for the three blocks sensitive to water vapour in shown in Figure 10; these are close ups of the top right
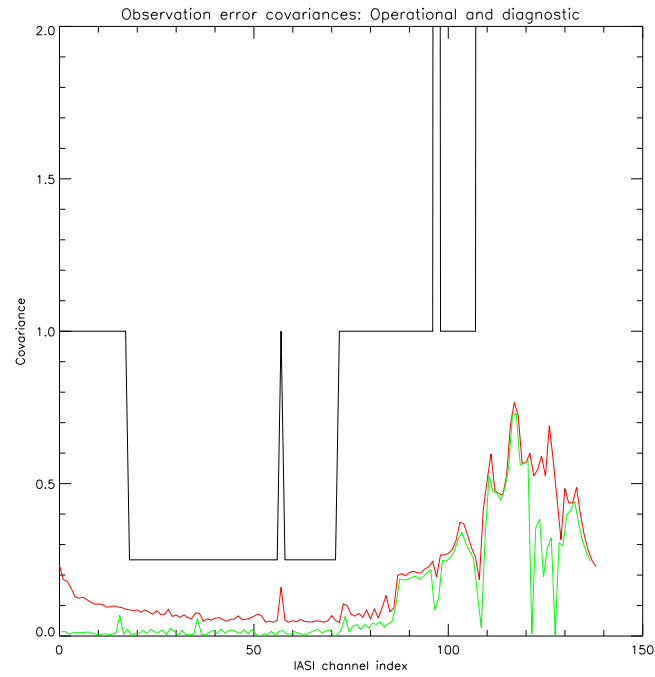
15

Figure 9: Operational error variances (black line), diagnosed error variances (red line), and first off-diagonal error covariance (green line)
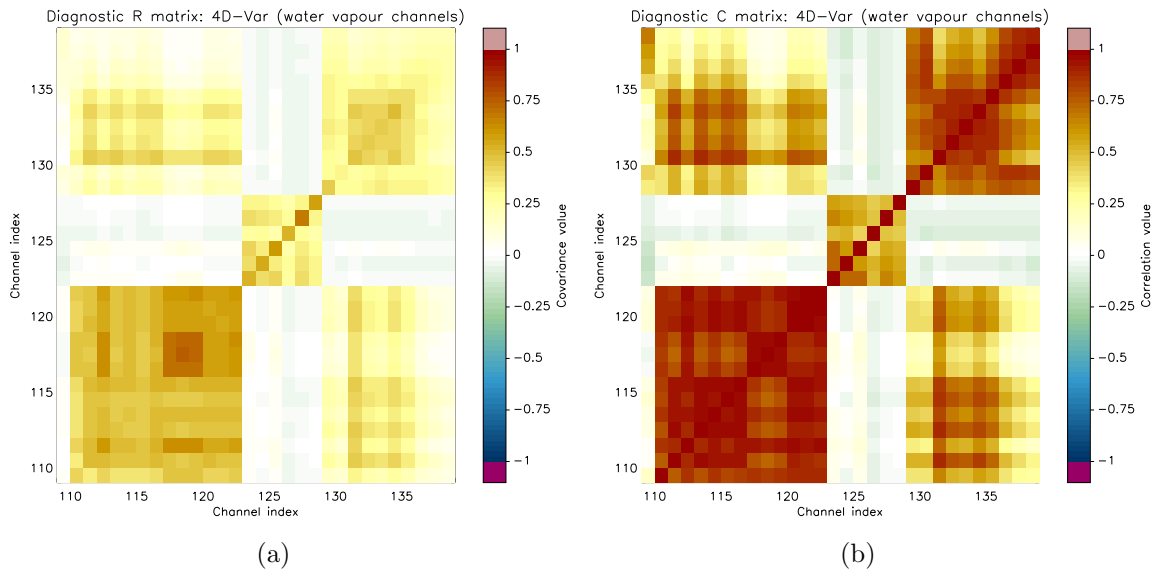

Figure 10: (a) Diagnosed observation error covariances in channels highly sensitive to water vapour; (b) diagnosed observation error correlations in channels highly sensitive to water vapour

corner of the plots in Figure 6. Again we see that the sizes of the off-diagonal covariances in the three blocks, are comparable with the diagonal variances. For an individual channel, the summed off-diagonal contributions are large enough to require a diagonal variance inflation if they are to be ignored. However, if we were to include some correlation structure in the observation error covariance matrix, the required variance inflation should be lower.

7 Conclusions

Using post analysis diagnostics derived from variational data assimilation theory, we can obtain information on the structure of the observation error covariance matrix under the assumptions of an optimal analysis. The infomation is derived using statistics on the background and analysis innovations of IASI brightness temperature measurements from 1D- and 4D-Var assimilation. Comparisons can be made with the current operational observation error covariances.

The application of the diagnostics to both the 1D- and 4D-Var assimilation procedures records observation error variances considerably smaller than those currently being used operationally. The statistics from the 1D-Var assimilation identify predominantly uncorrelated errors between channels, with some weak correlation in those channels sensitive to water vapour. However, the statistics from the 4D-Var assimilation show large off-diagonal error covariances in channels highly sensitive to water vapour, and additional correlation structure in channels in the temperature sounding band. These findings suggest that correlated observation errors in IASI data can largely be attributed to errors of representativity. Currently, all observation errors are assumed uncorrelated in the variational data assimilation performed at the Met Office; these results highlight the inconsistentcy of this assumption for IASI data.

Observation error correlations are shown to be significant between neighbouring channels with similar spectral properties, leading to a block structure in the error covariance and correlation matrix. A major issue with including observation error correlation structure in data assimilation algorithms is the inversion of a non-diagonal full observation error covariance matrix. If we could make the assumption that error correlation structure was in the block form as demonstrated here, the inversion problem is slightly simplified; the inverse of a matrix with a purely diagonal block structure is simply a block diagonal matrix of the inverses of the blocks. Additional assumptions can be made for individual blocks, to make their inversion suitably simple.

The diagnosed values of observation error covariances and correlations generated here, provide a realistic starting point for future work on including observation error correlation structure in variational data assimilation. Although the diagnosed matrices are not entirely symmetric, the data provides us with an approximation of the 'true' correlation structure, and an approximating symmetric matrix (10) can be generated. Against this we can therefore test any approximate error correlation

17

structures by examining features such as information content and analysis accuracy. The ability to include observation error correlation structure is vital if we are to further improve our utilisation of satellite data.

Appendix A

All the details given in this section are given by Fiona Hilton (personal communication). The tables below contain information on the 314 IASI channels stored in the Met Office database (MetDB).

The column entries are described here:

1. MetDB channel number: the channel number out of 314 stored in the MetDB

2. OPS index number: the index of the MetDB channel, out of 183, used in the OPS (starting at 0)

3. Var index number: the index of the MetDB channel, out of 139, used in 4D-Var (starting at 0)

4. Central wave number of the channel

5. Q jac peak (hPa): the pressure level at which the water vapour Jacobian peaks [8]

6. Summed Q jac peak: the sum over all model pressure levels of the absolute value of the water vapour jacobian, normalised by the maximum of the totals for the 314 MetDB channels (out of 1)

MetDB channel number	OPS index number	Var index number	Central wave number	Q jac peak (hPa)	Summed Q jac
1	0		648.50	0.36	0
2	1	0	654.25	0.36	0
3	2		657.00	0.45	0
4	3	1	657.50	0.45	0
5	4		658.50	2.06	0
6	5	2	659.00	1.36	0.001
7	6		659.50	1.36	0.003
8	7		660.60	1.09	0
9	8	3	660.50	0.36	0
10	9		661.25	0.29	0
11	10		662.25	2.04	0
12	11		662.75	0.87	0
13	12		663.25	0.87	0
14	13		664.50	1.66	0
15	14		665.00	0.29	0
16	15		665.50	0.70	0
17	16		666.00	1.09	0
18	17		666.50	2.06	0
19	18		667.00	0.45	0
21	19		668.50	0.70	0
22	20		669.00	0.70	0
23	21		669.50	0.56	0
24	22		670.00	0.87	0
25	23		670.75	14.81	0
26	24		671.25	0.87	0
27	25	4	672.00	1.09	0
28	26		672.50	0.45	0
29	27		673.00	2.51	0
30	28	5	673.75	0.87	0
31	29		674.50	0.22	0
32	30	6	675.25	0.56	0
33	31		676.00	1.36	0
34	32	7	676.75	1.36	0
35	33		677.50	1.09	0
36	34		678.00	0.36	0
37	35	8	678.50	0.87	0
38	36		679.25	1.36	0
39	37	9	680.00	1.36	0
40	38		680.75	0.29	0

MetDB channel number	OPS index number	Var index number	Central wave number	Q jac peak (hPa)	Summed Q jac
41	39		681.25	1.09	0
42	40	10	681.75	0.22	0
43	41		682.50	0.45	0
44	42	11	683.25	0.17	0
45	43		684.00	0.29	0
46	44		684.50	0.87	0
47	45	12	685.00	0.70	0
48	46		685.50	0.56	0
49	47	13	686.50	0.45	0
50	48		687.25	0.87	0
51	49	14	688.00	0.87	0.002
52	50		688.75	1.36	0.001
53	51	15	689.50	1.09	0.001
54	52	16	689.75	0.87	0
55	53	17	691.00	0.17	0
56	54	18	691.50	0.70	0
57	55	19	693.00	0.87	0
58	56	20	694.50	321.50	0.001
59	57	21	696.00	269.65	0.001
60	58	22	696.50	269.65	0.001
61	59	23	697.25	339.39	0
62	60	24	697.75	269.65	0.006
63	61	25	698.25	286.60	0.002
64	62	26	699.00	416.40	0
65	63	27	699.50	396.81	0
66	64	28	700.25	321.50	0
67	65	29	700.75	339.39	0
68	66	30	701.25	436.95	0
69	67	31	702.25	321.50	0
70	68	32	702.75	358.28	0
71	69	33	703.75	303.55	0.009
72	70	34	704.50	478.54	0.003
73	71	35	705.25	339.39	0.047
74	72	36	705.50	339.39	0.053
75	73	37	706.25	436.95	0.006
76	74	38	707.00	358.28	0.016
77	75	39	707.75	416.40	0.025
78	76	40	708.25	478.54	0.004
79	77	41	709.75	457.27	0.004
80	78	42	710.25	457.27	0.004
81	79	43	711.00	610.60	0.016

MetDB channel number	OPS index number	Var index number	Central wave number	Q jac peak (hPa)	Summed Q jac
82	80	44	711.50	610.60	0.005
83	81	45	712.00	610.60	0.005
84	82	46	713.50	358.28	0.103
85	83	47	714.75	638.60	0.022
86	84	48	715.25	610.60	0.009
87	85	49	718.25	457.27	0.004
88	86	50	718.75	457.27	0.002
89	87	51	719.50	377.05	0
90	88		720.50	0.45	0
91	89	52	721.25	543.05	0.004
92	90	53	725.50	727.44	0.038
93	91	54	726.50	759.16	0.123
94	92	55	727.00	727.44	0.026
95	93	56	728.50	696.97	0.032
96	94	57	731.00	478.54	0.478
97	95	58	731.50	610.60	0.092
98	96	59	732.25	727.44	0.113
99	97	60	733.25	727.44	0.022
100	98	61	733.75	759.16	0.096
101	99	62	734.75	727.44	0.023
102	100	63	736.25	727.44	0.022
103	101	64	737.50	727.44	0.062
104	102	65	738.00	727.44	0.048
105	103	66	738.50	759.16	0.121
106	104	67	739.00	727.44	0.076
107	105	68	739.50	727.44	0.054
108	106	69	740.00	727.44	0.175
109	107	70	740.50	416.40	0.223
110	108	71	741.25	543.05	0.008
111	109	72	742.00	696.97	0.08
112	110	73	744.25	610.60	0.426
113	111	74	745.00	610.60	0.413
114	112	75	745.75	759.16	0.215
115	113	76	746.50	759.16	0.178
116	114	77	747.25	759.16	0.237
117	115	78	748.25	610.60	0.224
118	116	79	748.75	759.16	0.344
119	117	80	751.25	759.16	0.132
120	118	81	751.75	759.16	0.288
121	119	82	752.75	727.44	0.188
122	120	83	753.25	727.44	0.188
123	121	84	754.50	610.60	0.496

MetDB channel number	OPS index number	Var index number	Central wave number	Q jac peak (hPa)	Summed Q jac
124	122	85	756.00	696.97	0.298
125	123	86	759.00	792.18	0.229
126	124	87	773.50	792.18	0.360
127	125	88	781.25	792.18	0.354
128	126	89	782.75	792.18	0.380
130	127	90	786.25	792.18	0.367
131	128	91	787.50	792.18	0.359
132	129	92	788.00	792.18	0.348
133	130		806.25	792.18	0.349
134	131	93	810.25	792.18	0.305
135	132	94	811.75	792.18	0.301
136	133	95	833.75	792.18	0.265
137	134	96	861.50	792.18	0.234
138	135	97	871.25	727.44	0.668
139	136	98	875.00	792.18	0.222
140	137	99	901.50	792.18	0.198
141	138		906.25	792.18	0.326
142	139		925.00	759.16	0.521
143	140	100	928.00	792.18	0.178
144	141		942.50	792.18	0.157
145	142	101	943.25	792.18	0.167
146	143	102	962.50	792.18	0.150
162	144		1091.25	696.97	0.528
163	145	103	1096.00	792.18	0.087
164	146	104	1115.75	826.58	0.088
165	147	105	1142.50	826.58	0.086
166	148		1149.50	610.60	0.694
167	149	106	1168.25	792.18	0.099
168	150		1174.50	377.05	0.896
170	151	107	1204.50	826.58	0.106
171	152	108	1206.00	727.44	0.485
176	153	109	1330.00	457.27	0.907
178	154	110	1367.00	610.60	0.947
179	155	111	1371.50	478.54	0.914
183	156	112	1380.75	610.60	0.951
184	157	113	1381.75	499.54	0.900

MetDB channel number	OPS index number	Var index number	Central wave number	Q jac peak (hPa)	Summed Q jac
185	158	114	1382.50	610.60	0.937
186	159	115	1384.25	499.54	0.942
189	160	116	1391.75	457.27	0.901
195	161	117	1401.50	436.95	0.899
196	162	118	1402.00	457.27	0.909
200	163	119	1408.00	478.54	0.942
201	164	120	1409.25	478.54	0.925
202	165	121	1410.75	478.54	0.911
215	166	122	1436.75	208.16	0.276
221	167	123	1456.75	208.16	0.231
251	168	124	1521.25	208.16	0.299
259	169	125	1539.00	208.16	0.257
261	170	126	1540.25	208.16	0.255
263	171	127	1542.00	208.16	0.269
270	172	128	1927.25	727.44	0.979
271	173	129	1986.75	727.44	0.887
272	174	130	1987.50	610.60	1.000
273	175	131	1989.50	638.60	0.967
274	176	132	1990.00	638.60	0.984
275	177	133	1990.50	610.60	0.973
276	178	134	1994.00	638.60	0.975
277	179	135	1994.50	727.44	0.912
278	180	136	1995.00	727.44	0.822
279	181	137	1995.50	759.16	0.748
280	182	138	1996.00	759.16	0.679

Appendix B

Consider a state vector x at time 0, whose true value is x_t and whose background estimate is x_b;

$$x_t = x_b + \epsilon^b,$$

where ϵ^b is the background error. The state vector can be evolved forward to time i under the tangent linear model $M(t_i, t_0) = M_i M_{i-1} \ldots M_2 M_1$, i.e, $x_i = M(t_i, t_0)x$. Consider n observations at n different times, where the observations are related to the state vector through the forward model H,

$$
\begin{aligned}
y_1 &= Hx_1 + \epsilon_1^o = HM_1 x_t + \epsilon_1^o \\
y_2 &= Hx_2 + \epsilon_2^o = HM_2 M_1 x_t + \epsilon_2^o \\
&\vdots \\
y_n &= Hx_n + \epsilon_n^o = HM_n \ldots M_2 M_1 x_t + \epsilon_n^o
\end{aligned}
$$

where y_1 is an observation at time 1, y_2 is an observation at time 2, etc, and ϵ_i^o is the observation error for y_i.

In 4D-Var assimilation, the observations, y_i, are combined with the background estimate, x_b, to produce an optimal analysis x_a, given by the solution of the cost function

$$J(x) = \frac{1}{2}(x - x_b)^T B^{-1}(x - x_b) + \frac{1}{2}\sum_{i=1}^{n}(y_i - Hx_i)^T R_i^{-1}(y_i - Hx_i)$$

where $R_i = \mathbb{E}\left[\epsilon_i^o (\epsilon_i^o)^T\right]$.

Assuming that the observation and background errors are uncorrelated, the above cost function can be rewritten in matrix form

$$J(x) = \frac{1}{2}(x - x_b)^T B^{-1}(x - x_b) + \frac{1}{2}(\mathbf{y} - \mathbf{h}x)^T R^{-1}(\mathbf{y} - \mathbf{h}x)$$

where

$$\begin{aligned}
\mathbf{y} &= (y_1^T, y_2^T, \ldots, y_n^T)^T, \\
\mathbf{h} &= (M_1^T H^T, M_1^T M_2^T H^T, \ldots, M_1^T M_2^T \ldots M_n^T H^T)^T, \\
\epsilon^o &= ((\epsilon_1^o)^T, (\epsilon_2^o)^T, \ldots, (\epsilon_n^o)^T)^T, \\
R = \mathbb{E}\left[\epsilon^o(\epsilon^o)^T\right] &= \mathbb{E}\left[\begin{pmatrix}
\epsilon_1^o(\epsilon_1^o)^T & \epsilon_1^o(\epsilon_2^o)^T & \ldots & \epsilon_1^o(\epsilon_n^o)^T \\
\epsilon_2^o(\epsilon_1^o)^T & \epsilon_2^o(\epsilon_2^o)^T & \ldots & \epsilon_2^o(\epsilon_n^o)^T \\
\vdots & \vdots & \ddots & \vdots \\
\epsilon_n^o(\epsilon_1^o)^T & \epsilon_n^o(\epsilon_2^o)^T & \ldots & \epsilon_n^o(\epsilon_n^o)^T
\end{pmatrix}\right] \\
&= \begin{pmatrix}
\mathbb{E}\left[\epsilon_1^o(\epsilon_1^o)^T\right] & 0 & \ldots & 0 \\
0 & \mathbb{E}\left[\epsilon_2^o(\epsilon_2^o)^T\right] & \ldots & 0 \\
\vdots & \vdots & \ddots & \vdots \\
0 & 0 & \ldots & \mathbb{E}\left[\epsilon_n^o(\epsilon_n^o)^T\right]
\end{pmatrix} \\
&= \begin{pmatrix}
R_1 & 0 & \ldots & 0 \\
0 & R_2 & \ldots & 0 \\
\vdots & \vdots & \ddots & \vdots \\
0 & 0 & \ldots & R_n
\end{pmatrix}.
\end{aligned}$$

This is the form of the cost function in 3D-Var data assimilation, and can be solved using the same approach, i.e, setting the cost function gradient to zero. The solution to the 4D-Var assimilation problem can therefore be described by

$$x_a = x_b + B\mathbf{h}^T(\mathbf{h}B\mathbf{h}^T + R)^{-1}(\mathbf{y} - \mathbf{h}x_b).$$

References

[1] H. Berger and M. Forsythe. Satellite wind superobbing. *Met Office Forecasting Research Technical Report*, 451, 2004.

[2] N. Bormann, S. Saarinen, G. Kelly, and J-N. Thepaut. The spatial structure of observation errors in Atmospheric Motion Vectors for geostationary satellite data. *Monthly Weather Review*, 131.

[3] G. Chalon, F. Cayla, and D. Diebel. IASI: An advanced sounder for operational meteorology. In *Proceedings of IAF, Toulouse, France, 1-5 October, 2001*, 2001.

[4] A.D. Collard. Selection of IASI channels for use in Numerical Weather Prediction. *Q.J.R.Meteorol.Soc.*, 133.

[5] A.D. Collard. On the choice of observation errors for the assimilation of AIRS brightness temperatures: A theoretical study. *ECMWF Technical Memoranda*, AC/90, 2004.

[6] M.J.P. Cullen. The unified/forecast climate model. *Meteorol. Mag.*, 122:81–94.

[7] G. Desroziers, L. Berre, B. Chapnik, and P. Poli. Diagnosis of observation, background and analysis-error statistics in observation space. *Q.J.R.Meteorol.Soc.*, 131:3385–3396, 2005.

[8] J. Eyre. Inversion methods for satellite sounding data. In *Meteorological Training Course Lecture Series, ECMWF, Reading*, 2002.

[9] S.B. Healy and A.A. White. Use of discrete Fourier transforms in the 1D-Var retrieval problem. *Q.J.R.Meteorol.Soc.*, 131.

[10] A. Hollingsworth and P. Lonnberg. The statistical structure of short-range forecast errors as determined from radiosonde data. Part 1: The wind field. *Tellus*, 38A:111–136, 1986.

[11] A.S. Lawless, S. Gratton, and N.K. Nichols. An investigation of incremental 4D-Var using non-tangent linear models. *Q.J.R.Meteorol.Soc.*, 131:459–476, 2005.

[12] F. Rawlins, S.P. Ballard, K.J. Bovis, A.M. Clayton, D. Li, G.W. Inverarity, A. C. Lorenc, and T.J. Payne. The Met Office global four-dimensional variational data assimilation scheme. *Q.J.R.Meteorol.Soc.*, 133.

[13] C.D. Rodgers. Information content and optimisation of high resolution measurements. *Optical spectroscopic techniques and instrumentation for atmospheric and space research II*, pages 136–147, 1996.

[14] R. Saunders, P. Brunel, S. English, P. Bauer, U. O'Keeffe, P. Francis, and P. Rayer. RTTOV-8 science and validation report.

[15] L. Stewart, S. Dance, and N.K. Nichols. Correlated observation errors in data assimilation. *Int.J.Numer.Meth.Fluids*, 56:1521–1527, 2008.

[16] O. Talagrand. A posteriori verification of analysis and assimilation algorithms. In *Proceedings of Workshop on diagnosis of data assimilation systems, ECMWF, Reading, UK, 2-4 November 1998*, pages 17–28, 1999.